Journal of Alloys and Compounds 521 (2012) 101–105

Contents lists available at SciVerse ScienceDirect

Journal of Alloys and Compounds

journal homepage: www.elsevier.com/locate/jallcom

Magnetic properties of chemical coprecipitated $Sr_{0.8}La_{0.2}Fe_{11.8}Co_{0.2}O_{19}$ powders

C. Serletis [a], G. Litsardakis [b], E.K. Polychroniadis [a], K.G. Efthimiadis [a,*]

[a] Department of Physics, Aristotle University, Thessaloniki 54124, Greece
[b] Department of Electrical & Computer Engineering, Aristotle University, Thessaloniki 54124, Greece

ARTICLE INFO

Article history:
Received 7 November 2011
Received in revised form 9 January 2012
Accepted 9 January 2012
Available online 28 January 2012

Keywords:
Sr-hexaferrite
La–Co substitution
Chemical coprecipitation
Permanent magnets
Anisotropy field
Activation volume

ABSTRACT

For this work, $Sr_{0.8}La_{0.2}Fe_{11.8}Co_{0.2}O_{19}$ hexaferrite powders were manufactured, using the chemical co-precipitation method. Major and minor magnetization loops recorded at room temperature show that the optima hard magnetic properties are achieved when the calcination temperature is 1000 °C. SEM, TEM and XRD measurements show that the 1000 °C calcined powder consists of single hexaferrite phase fine particles with a mean diameter of 90 nm. From remanence magnetization, coercivity, magnetic viscosity and irreversible susceptibility measurements there can be concluded that the powder consists of single domain magnetic particles of platelet shape.

1. Introduction

La–Co substituted Ba- or Sr-hexaferrites are high-performance permanent magnets that are expected to enter the market when the performance/price ratio is optimized by reducing the manufacturing cost, which is high due to the use of the more expensive rare earth elements in the process [1].

Their characterization as high-performance permanent magnets comes from the fact that they present, compared to conventional hexaferrites, both stronger magnetocrystalline anisotropy and thus a stronger coercive field and a more stable thermal dependence of their magnetic properties (reduced thermal coefficient of H_c). Their magnetic properties are qualitatively interpreted based on micromagnetic models, but there is still some research interest [2–7], focused on the development of a cheaper manufacturing process that will not affect the enhanced magnetic properties of these materials.

During this effort in the last decade, La–Co substituted Sr-hexaferrites were manufactured with the chemical co-precipitation method. The advantage of this particular method is that the final product is a fine particle powder and thus no milling is required in the manufacturing process. But the magnetic properties of these hexaferrites have not yet been fully studied, particularly the implications of the small particle size.

In this work, we manufactured a $Sr_{0.8}La_{0.2}Fe_{11.8}Co_{0.2}O_{19}$ fine particle powder with the chemical co-precipitation method and extensively studied their magnetic properties, in order to determine the magnetization reversal mechanisms.

2. Chemical preparation

Initially, an aqueous solution of the chemical precursors $Sr(NO_3)_2$, $La(NO_3)_3{\cdot}6H_2O$, $Fe(NO_3)_3{\cdot}9H_2O$ and $Co(NO_3)_2{\cdot}6H_2O$ was mixed. The precursors' mass was calculated so that the ratio $[Sr^{2+} + La^{3+}]/[Fe^{3+} + Co^{2+}]$ was equal to 1/12, corresponding to the composition of $Sr_{0.8}La_{0.2}Fe_{11.8}Co_{0.2}O_{19}$. The solution was then infused to an aqueous solution of NaOH with excessive sodium hydroxide so that the ratio $[NO_3^-]/[OH^-]$ was equal to 1/2. The final solution was stirred at 700 rpm for 2 h at 130 °C and filtered. The precipitate was washed and dried for 19 h at 110 °C.

3. Calcination procedure

A 2-h calcination procedure in air was used for the formation of the hexaferrite phase, at 5 different temperatures (900 °C, 1000 °C, 1100 °C, 1150 °C, 1200 °C), in order to achieve the best hard magnetic properties. So, before any chemical or structural characterization of the materials was attempted, a first magnetic characterization at room temperature was made, using a vibrating sample magnetometer (P.A.R. 155).

In Fig. 1, the magnetization at 2 T, the remanence magnetization and the coercive field of the materials at room temperature are presented in relation with the calcination temperature. These

* Corresponding author. Tel.: +30 2310998065; fax: +30 2310998003.
E-mail address: kge@auth.gr (K.G. Efthimiadis).

0925-8388/$ – see front matter © 2012 Elsevier B.V. All rights reserved.
doi:10.1016/j.jallcom.2012.01.055

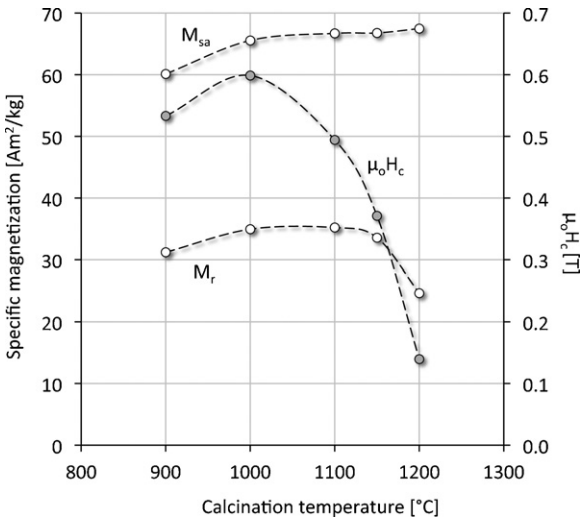

Fig. 1. Magnetization at 2 T (M_{sa}), remanence magnetization (M_r) and coercive field (H_c) of samples vs calcination temperatutre.

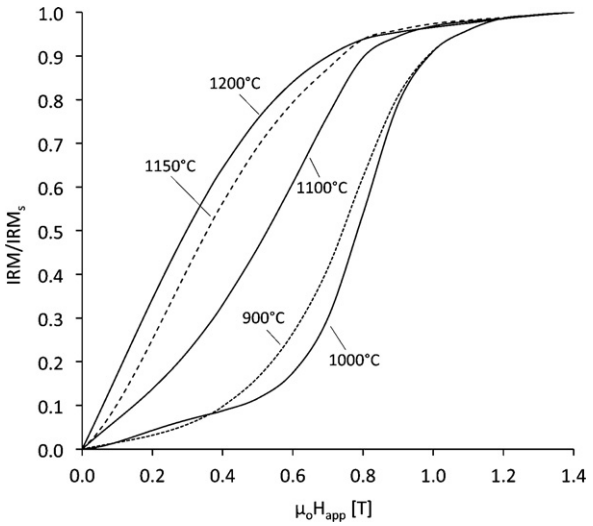

Fig. 3. Field dependency of the initial remanence magnetization (IRM) of samples with different calcination temperatures. IRM_s is the maximum remanence magnetization of the samples.

results were derived from the recording of major magnetization loops (Fig. 2). As shown, the best results concerning hard magnetic properties are achieved with a calcination temperature of 1000 °C.

The magnetic behavior of materials during their initial magnetization (the increase of remanence magnetization and coercive field in relation to the external applied field) is shown in Figs. 3 and 4. These results were derived from the recording on minor hysteresis loops, reduced to the respective saturation values. Based on the work of Hadjipanayis et al. [8] about the magnetization reversal in ferrite magnets, the samples calcined at 1000 °C show the best approximation to the fine particle magnetization behavior.

Finally, Henkel plots of each sample (the tracing of remanence magnetization during a dc demagnetization, DCD, in relation to the remanence magnetization during the initial magnetization, IRM) are presented in Fig. 5. The curves are reduced to the respective saturation magnetization (DCD_s, IRM_s). From these experimental results, we derive qualitative conclusions concerning the interactions between magnetic particles [8–13]. For non-interacting particles, this plot is linear [10]. Materials calcined at 1000 °C show a strong negative deviation from linearity, which indicates that they consist of magnetic particles with dipole magnetic interactions.

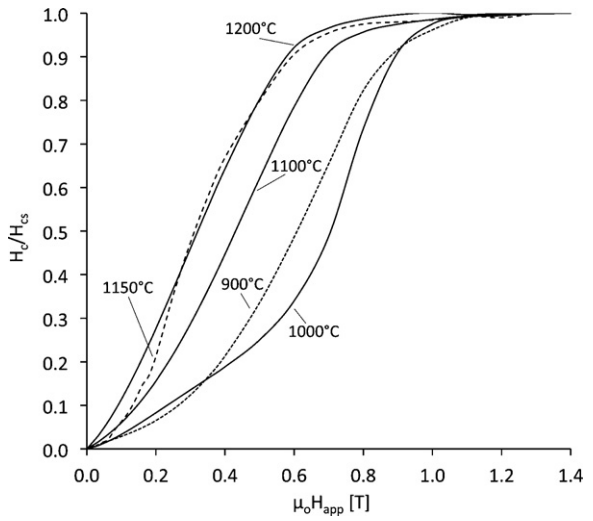

Fig. 4. Field dependency of the coercive field (H_c) of samples with different calcination temperatures. H_{cs} is the maximum coercive field of the samples.

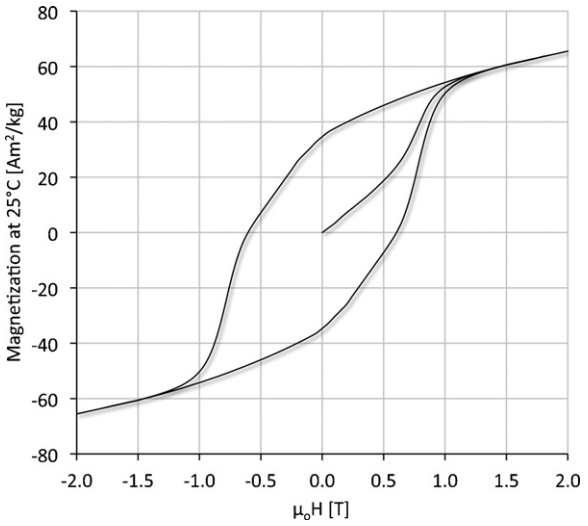

Fig. 2. Major hysteresis loop for the 1000 °C calcined sample.

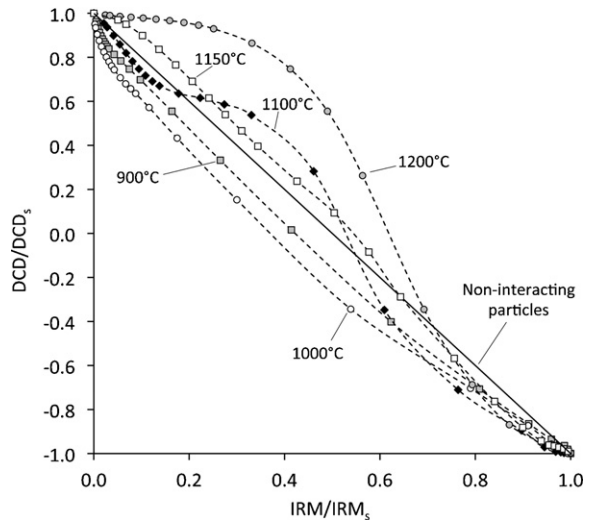

Fig. 5. Henkel plots of samples with different calcination temperatures.

Table 1
Nominal and measured atomic composition of the 1000 °C calcined sample.

	Nominal (at.%)	SEM/EDAX (at.%)
O	59.4	60.3
Fe	36.9	36.1
Co	0.6	0.5
Sr	2.5	2.4
La	0.6	0.7

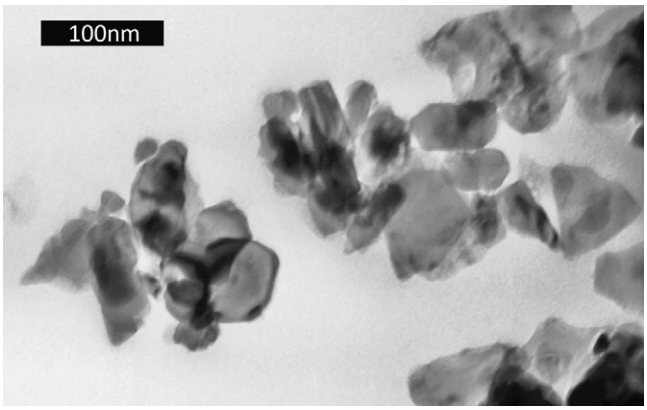

Fig. 6. TEM image of the 1000 °C calcined particles.

In summary, this initial magnetic characterization shows that the optimum calcination temperature is 1000 °C, thus the following study was limited to this material.

4. Chemical and structural characterization

The atomic composition of the 1000 °C calcined material was evaluated by means of a JEOL JSM 5900 LV scanning electron microscope, equipped with an INCA x-sight detector (Oxford Instruments) for energy dispersive X-ray microanalysis. The results (Table 1) show small deviations from the nominal composition of $Sr_{0.8}La_{0.2}Fe_{11.8}Co_{0.2}O_{19}$ hexaferrite.

Because the microstructural observation with SEM showed clumps of small particles, a JEOL JEM 120CX transmission electron microscope with 120 kV operating voltage was used to determine the size of particles. In the TEM images (Figs. 6 and 7) the particle size is shown, and a size distribution of 172 measured particles is shown in Fig. 8. Fitting with a log-normal probability distribution function estimates the particles' mean diameter equal to 90 nm.

X-ray patterns were obtained by a powder diffractometer (Seifert XRD-3003TT), using Fe K_α radiation, and they were identified according to the relevant JCPDS-ICDD Powder Diffraction Files.

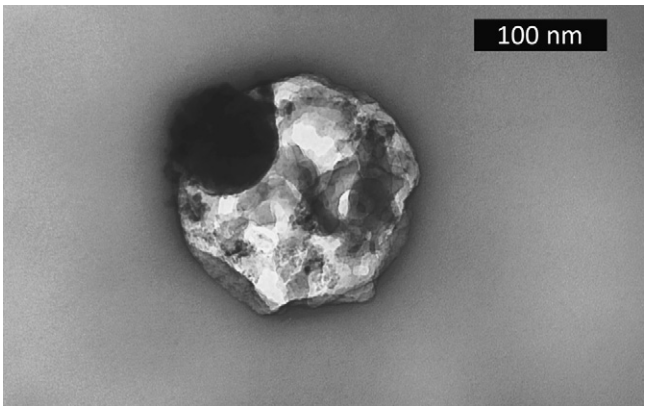

Fig. 7. TEM image of an isolated 1000 °C calcined particle.

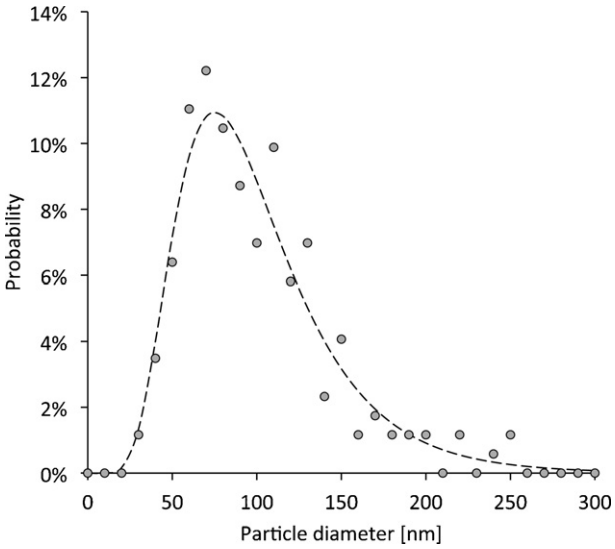

Fig. 8. Distribution of particle size in the 1000 °C calcined powder.

The examination of X-ray diffraction diagram of sample calcined at 1000 °C shows that only the hexaferrite structure is formed (Fig. 9). Peaks are typically indexed as M-type hexaferrite (space group $P6_3/mmc$, $a = 5.875$ Å and $c = 23.015$ Å), according to JCPDS Card 84-0757.

The use of the Scherrer equation evaluates the diameter of particles around 60 nm, using data from the 5 most intensive peaks, less than the diameter evaluated from TEM measurements. According to micromagnetic calculations [4,5], the critical diameter for single domain particles is estimated above 600 nm, so the material under study can be characterized as a single domain particle powder.

5. Thermal dependence

In Fig. 10 there are shown experimental results concerning the thermal dependence of the magnetization at 2 T and of the remanence magnetization. Also shown is the thermal dependence of the saturation magnetization (M_s), as calculated from fitting the experimental data to the relation $M = M_s - a/H - b/H^2$. The necessity of the second and third term of the equation ($1/H$, $1/H^2$) was proven equally important for the fitting of the experimental data, with a correlation coefficient greater than 0.999. It must be noted that in these calculations no less than 12 points were used from the part of

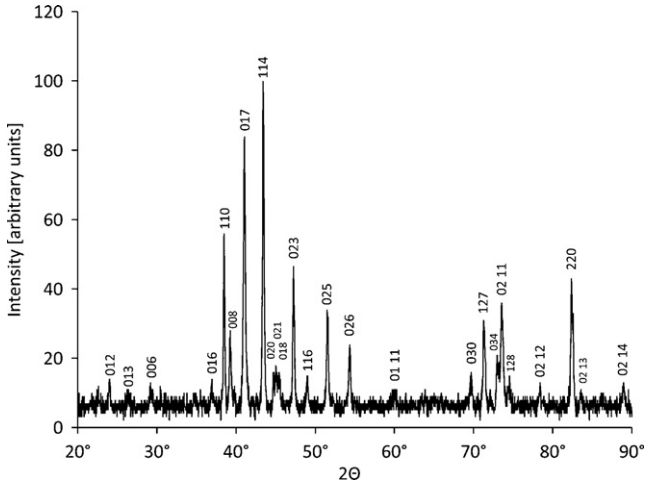

Fig. 9. XRD pattern of the 1000 °C calcined powder.

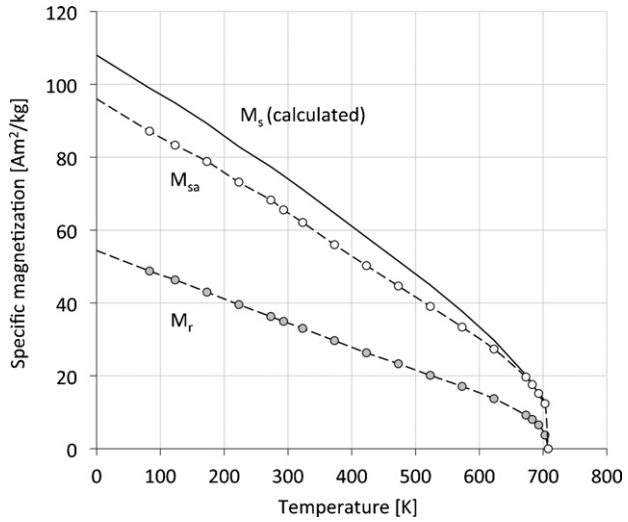

Fig. 10. Temperature dependency of the magnetization at 2 T (M_{sa}), remanence magnetization (M_r) and calculated saturation magnetization (M_s) in the 1000 °C calcined powder.

M–H loop, in which magnetization displays a reversible behavior. According to the fitting's results, specific saturation magnetization at room temperature is 75 Am^2/kg, while by extrapolating from liquid nitrogen temperature to 0 K, specific saturation magnetization is 108 Am^2/kg. The Curie temperature of the material is 705 K.

The remanence magnetization at room temperature is 35 Am^2/kg, while at 0 K it is estimated at 54 Am^2/kg. The ratio M_r/M_s is equal to 0.5 at 0 K and is reduced with increasing temperature: at room temperature it is 0.47 and at 700 K 0.40. This phenomenon is an indication that the material consists of non-oriented single domain magnetic particles, in which this ratio is theoretically 1/2 and reduces with increasing temperature due to thermally activated magnetization reversal.

Fig. 11 shows the temperature dependence of the coercive and anisotropy field. The latter was assumed to be the external applied field where the branches of a magnetization loop are united, meaning that irreversible processes of magnetization reversal have either been completed during magnetization, or initiated during demagnetization. These results are further validated by the SPD method, which produces a local maxima in the second derivative $|d^2M/dH^2|$. From experimental data (Figs. 3 and 4) it is also concluded that during the material's magnetization under that field, both remanence magnetization and coercive field saturate.

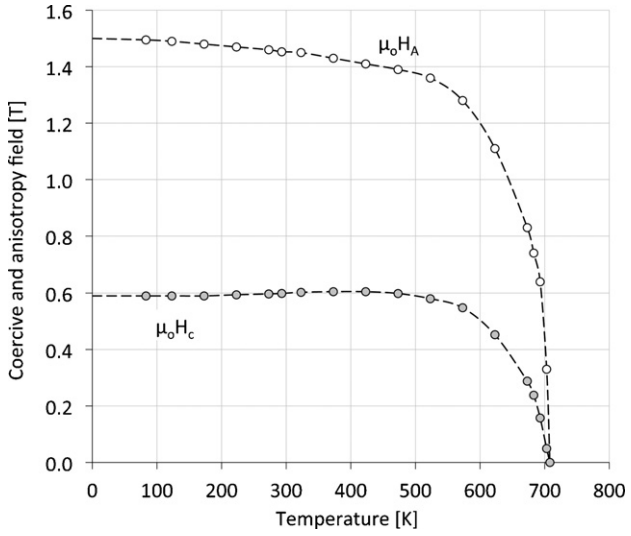

Fig. 11. Temperature dependency of the coercive (H_c) and anisotropy field (H_A) in the 1000 °C calcined powder.

According to these measurements, at room temperature the anisotropy field is 1.45 T. Using the SPD method, Tenaud et al. [14] determine the anisotropy field to be 2.17 T in hexaferrites of the same chemical composition, but different microstructure. They used the ceramic manufacturing process, which produces crystallites with bigger size and different shape. As we explain in the following paragraph, this difference in experimental results can be attributed to the crystallites shape anisotropy.

In micromagnetism theory, anisotropy field is given by the relation $\mu_o H_A = 2K/dM_s - N\mu_o dM_s$, where K [J/m^3] is the magnetocrystalline anisotropy coefficient, M_s [Am^2/kg] the specific saturation magnetization, d [kg/m^3] the density of particles and $N = N_{||} - N_{\perp}$ the demagnetization factors of particles, parallel and perpendicular to the easy axis. Density can be calculated by the relation $d = d_o/(1+\alpha\Delta T)^3$, where $d_o = 5178\ kg/m^3$ is the density at room temperature, as calculated from the dimensions and composition of the unit cell and $\alpha \approx 10^{-5}\ K^{-1}$ [15] a typical value for the linear thermal expansion coefficient of hexagonal ferrites. The magnetocrystalline anisotropy coefficient for Sr-hexaferrite single crystals was measured at 350 kJ/m^3 [16]. By replacing this value in the aforementioned relation, factor N equals 0.72, while for a slightly bigger value ($K = 375\ kJ/m^3$, as normally expected for La–Co substituted Sr-hexaferrites), N approaches 1. This means that in the materials under study shape anisotropy is strong, because such values for N only appear in single domain particles with platelet shape. This particle shape is generally obtained in M-type hexaferrites prepared by chemical methods [17]. The effect of shape anisotropy competes with the effect of magnetocrystalline anisotropy, thus reducing the effective anisotropy field.

Concerning the coercive field, experimental data are perfectly fitted to the relation $\mu_o H_c = 0.48\mu_o H_A - 0.17\mu_o d' M_s$, where d' is the packed powder density, estimated lower than the density of particles due to the space between them and equal to $5000/(1+\alpha\Delta T)^3\ kg/m^3$. Qualitatively the coefficient 0.48 is mainly attributed to the fact that the sample consists of non-oriented magnetic particles, while the additional term ($0.17\mu_o d' M_s$) is attributed to local stray fields due to the space between particles.

6. Irreversible magnetization processes

Fig. 12 shows magnetic viscosity and irreversible susceptibility measurements related to the external applied field during demagnetization from saturation. Magnetic viscosity was measured from its definition relation $S = \Delta M/\Delta\ln(t)$, where ΔM is the magnetization change under constant applied field and temperature, in a time frame ranging from 100 s to 10,000 s after the stabilization of the applied field. Irreversible susceptibility was calculated from the relation $\chi_{irr} = \chi_{tot} - \chi_{rev}$, where $\chi_{tot} = dM/dH$ is the differential susceptibility during the demagnetization from saturation, while χ_{rev} is the susceptibility in a small reduction of the demagnetizing applied field. Both quantities concern irreversible magnetization processes, the first due to thermal activations and the second due to field activations. They present similar behavior related to the applied field and show a maximum at 0.7 T, higher than the coercive field (0.6 T).

Using the relation field $v_a = KT\chi_{irr}/\mu_o dM_s S$ [m^3], the activation volume of magnetization reversal can be calculated from the aforementioned experimental data. In Fig. 13 the size of the volume is shown, considering it as a cube. The volume is almost independent of the applied field and approximately averages $22^3\ nm^3$.

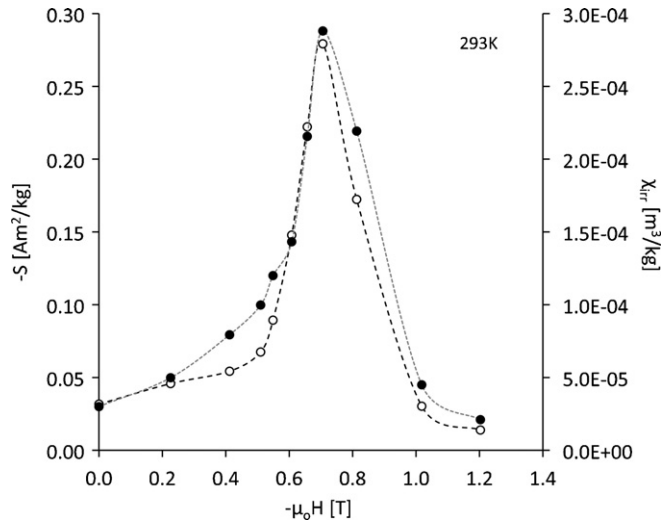

Fig. 12. Magnetic viscosity (S, white circles) and irreversible susceptibility (χ_{irr}, black circles) at various demagnetization fields at room temperature.

Magnetic viscosity, irreversible susceptibility and activation volume present the same behavior in higher temperatures. Fig. 14 shows the thermal dependence of activation volume, reaching 42^3 nm^3 near the Curie temperature.

It is worth noting that the activation volume is smaller than the particles' volume. Ding et al. [18] noticed the same phenomenon in single domain Ba- and Sr-hexaferrite particles prepared by mechanical alloying. In 300 nm diameter particles they calculated the activation volume to be equal to a sphere of 25 nm diameter.

Provided that the analysis of our experimental results points to the conclusion that the material consists of single domain particles, the mechanism of magnetization reversal is coherent irreversible rotation and in this case, activation volume should be equal to particle volume. This discrepancy could be attributed to two computational errors. The first concerns the activation volume calculation relation. This relation applies for an easy-axis oriented material, where the dependence of energy barriers from the interacting field is $\partial\Delta/\partial H = \mu_o dM_s v_a$. The term $\mu_o dM_s$ is placed in the denominator. For non-oriented particles, this term should be smaller, because for each misaligned particle it should be multiplied with the cosine of the angle between the easy axis and the direction in the interacting field, so the activation volume for non-oriented particles is always larger than the one calculated from the aforementioned relation. The second error concerns the particles' shape. If a volume of 22^3 nm^3 corresponds to a platelet shape, then 2 of the 3 particle's dimensions are larger and comparable to 60 and 90 nm calculated from XRD and TEM measurements, respectively.

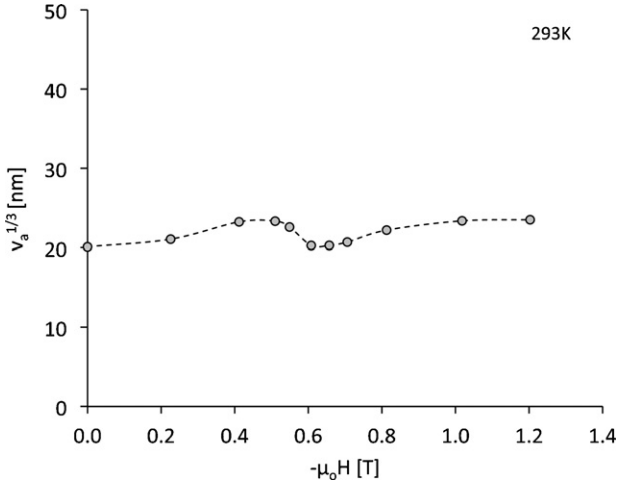

Fig. 13. Size of the activation volume at various demagnetization fields.

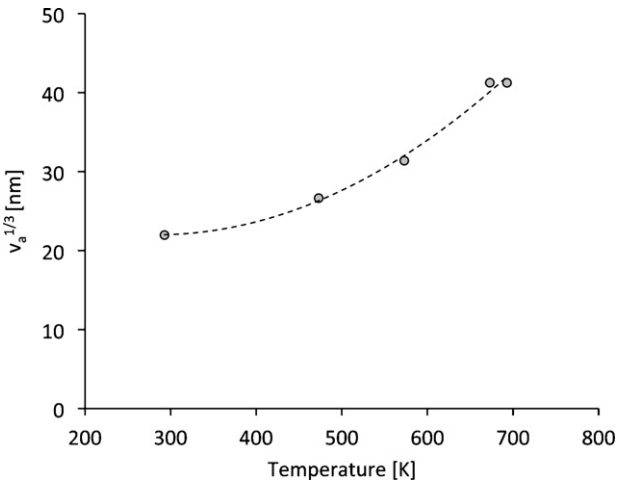

Fig. 14. Mean size of the activation volume at various temperatures.

7. Conclusions

From TEM, XRD and magnetic measurements in $Sr_{0.8}La_{0.2}Fe_{11.8}Co_{0.2}O_{19}$ hexaferrites prepared by chemical coprecipitation, it is concluded that the material consists of single domain magnetic particles with dipole magnetic interactions. They exhibit strong uniaxial magnetocrystalline anisotropy and also a strong anisotropy due to their platelet shape. The latter competes with the former, weakening the hard magnetic properties of the material.

If the manufacturing process is optimized so that the particles' shape is more uniform, then permanent magnets with very large coercive field could be constructed by orienting the powder.

References

[1] F. Kools, A. Morel, R. Grössinger, J.M. Le Breton, P. Tenaud, J. Magn. Magn. Mater. 242–245 (2002) 1270.
[2] J.M. Le Breton, J. Teillet, G. Wiesinger, A. Morel, F. Kools, P. Tenaud, IEEE Trans. Magn. 38 (2002) 2952.
[3] J.F. Wang, C.B. Ponton, R. Grössinger, I.R. Harris, J. Alloys Compd. 369 (2004) 170.
[4] Z. Pang, X. Zhang, B. Ding, D. Bao, B. Han, J. Alloys Compd. 492 (2010) 691.
[5] H. Nishio, Y. Minachi, H. Yamamoto, IEEE Trans. Magn. 45 (2009) 5281.
[6] J-M. Le Breton, L. Lechevallier, J.F. Wang, R. Harris, J. Magn. Magn. Mater. 272–276 (2004) 2214.
[7] H. Yamamoto, H. Seki, IEEE Trans. Magn. 35 (1999) 3277.
[8] G.C. Hadjipanayis, E.W. Singleton, Z.X. Tang, J. Magn. Magn. Mater. 81 (1989) 318.
[9] O. Henkel, Phys. Status Solidi 7 (1964) 919.
[10] E.P. Wohlfarth, J. Appl. Phys. 29 (1958) 595.
[11] G.W.D. Spratt, P.R. Bisell, R.W. Chantrell, E.P. Wohlfarth, J. Magn. Magn. Mater. 75 (1988) 309.
[12] J. García-Otero, M. Porto, J. Rivas, J. Appl. Phys. 87 (2000) 7376.
[13] Q. Chen, B.M. Ma, B. Lu, M.Q. Huang, D.E. Laughlin, J. Appl. Phys. 85 (1999) 5917.
[14] P. Tenaud, A. Morel, F. Kools, J.M. Le Breton, L. Lechevallier, J. Alloys Compd. 370 (2004) 331.
[15] H. Kojima, Fundamental properties of hexagonal ferrites, in: E.P. Wohlfarth (Ed.), Ferromagnetic Materials, vol. 3, North-Holland Publishing Company, 1982, p. 363.
[16] L. Jahn, H.G. Müller, Phys. Status Solidi 35 (1969) 723.
[17] M. Jean, V. Nachbaur, J. Bran, J.-M. Le Breton, J. Alloys Compd. 496 (2010) 306.
[18] J. Ding, R. Street, H. Nishio, J. Magn. Magn. Mater. 164 (1996) 385.